Power Electronic Systems
Laboratory

Proceedings of the IEEE Energy Conversion Congress and Exposition (ECCE USA 2011), Phoenix, USA,
September 18-22, 2011.

PEEC-based Virtual Design of EMI Input Filters

I. Kovacevic
T. Friedli
A. Müsing
J.W. Kolar

Eidgenössische Technische Hochschule Zürich
Swiss Federal Institute of Technology Zurich

PEEC-based Virtual Design of EMI Input Filters

Ivana F. Kovačević, Thomas Friedli, Andreas Müsing and Johann W. Kolar
Swiss Federal Institute of Technology, ETH Zurich
Power Electronic Systems Laboratory
Zurich, 8092 Switzerland
kovacevic@lem.ee.ethz.ch

***Abstract*—The paper summarizes a step by step Partial Element Equivalent Circuit (PEEC) modeling approach for Electro-magnetic Interference (EMI) filter components (e.g. foil capacitors, common mode and differential mode inductors) and PCB tracks, to design complete EMI input filters with an optimal selection and placement of the individual components. The presence of magnetic cores is modeled with the proposed PEEC-Boundary Integral Coupled Method (PEEC-BIM) by means of fictitious magnetic surface currents, using the core geometry and permeability as inputs. The developed PEEC based models are verified by transfer function measurements of several single-phase single/two-stage filter circuits. The resulting PEEC simulation time is determined by the time required to perform the surface mesh of the magnetic volume and is in the order of several minutes. The good results of the presented PEEC modeling approach enable a fast virtual design of EMI filters and help to accelerate the design process of power converter systems.**

Keywords - EMC, EMI filter components, parasitic effects, mutual coupling, Partial Element Equivalent Circuit (PEEC) Method.

I. INTRODUCTION

To prevent EMI problems from causing the malfunctioning of Power Electronic (PE) systems, the prediction of Electro-Magnetic (EM) behavior of the overall PE system is essential and should ideally be considered in the earliest system design stage. Therefore, in order to avoid Electro-Magnetic Compatibility (EMC) problems, the main task is the design of EMI input filter circuits which provide the necessary insertion loss in the whole frequency range of interest (typically from 150 kHz to 30 MHz) [1]. With high integration density of PE systems, system optimization concerning e.g. volume and cost aspects has to be performed. Three-dimensional modeling facilitating the optimization procedure turns out to be a necessary design approach. Thus far, a major limitation in this context was the modeling of the stray field of passive PE components generated by both common (CM) and differential (DM) mode EMI propagation signals of the line-connected equipment [2]. Therefore, the development and implementation of 3D models of passive PE components based on the Partial Element Equivalent Circuit (PEEC) method is addressed in this paper.

The Partial Element Equivalent (PEEC) method has often been the numerical technique of choice for the modeling of interconnections such as bus-bars, PCBs etc [3]. Accordingly, the presented research is focused on the PEEC-based modeling of EMI input filters based on the previously developed PEEC-Boundary Integral (PEEC-BIM) method [4]. The PEEC simulation results enable a comprehensive insight into the EM characteristics of the EMI filter prior to the construction of the final filter hardware prototype. Taking into account the influence of both parasitic and mutual coupling effects [7, 8], multilevel prediction of the EMI filter performance is enabled [6]. The detailed 3D-PEEC models of the filter capacitors and CM/DM inductors are developed including both their self and stray characteristics. Compared to previously published work [9-11], the 3D model of the EMI filter inductors is developed including the presence of the magnetic core by means of the proposed PEEC-BIM coupled method without any geometrical simplifications [10, 11] and the effective permeability assumption [9].

II. STATE OF THE ART-PEEC METHOD

The PEEC method has proven to be a convenient modeling approach for circuit-field coupled problems such as PCB layouts, and EMI filters of power converters. The PEEC method is derived from Maxwell's integral equations in the form of Kirchhoff's laws (Fig. 1) so that the PEEC models can be easily combined with any circuit-solver e.g. *GeckoCIRCUIT* [12].

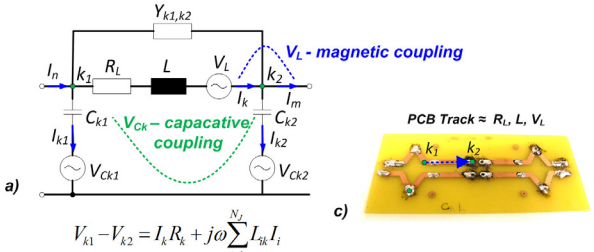

Fig. 1. a) PEEC equivalent circuit of a PCB example; b) PEEC circuit equations; c) Photo of a PCB.

As only the mesh of conducting, dielectric and magnetic volumes is required, the PEEC method reduces the computational complexity compared to the Finite Element Method (FEM) especially in the 3D case of PE systems comprising many interconnections and circuit elements of quite different geometrical dimensions.

The main challenge of PEEC-based modeling is the presence of non-homogeneous and nonlinear magnetic materials. This has previously adversely affected the PEEC modeling of magnetic core inductors. However, the

linearization of magnetic properties by means of the relative permeability, μ_r, enables the extension of PEEC to 3D modeling in the presence of magnetic materials and, further, the development of an accurate PEEC model of EMI filter inductors. The PEEC-Boundary Integral Method (PEEC-BIM) was first proposed in [4] for modeling toroidal inductors in the frequency domain. The simplified PEEC-BIM method was then introduced in [5] showing that it can be used to accurately model both the self and stray properties of toroidal inductors which are typically used in EMI filter applications. In addition, the performance of the developed PEEC-BIM approach shows acceptable computation time.

III. PEEC-BIM Method Basic Theory

From EM theory, the magnetization **M** given in a magnetic volume, V_M, can be modeled by replacing V_M with an equivalent distribution of fictitious magnetic currents [13]. In the case of homogeneous linear magnetic material, only the surface S_M of V_M has to be considered lessening the problem to the calculation of only magnetic surface currents, $\mathbf{K_M}$. The permeability curves, $\mu_r(f)$, characterizing the linear properties of V_M, are either taken from datasheets or extracted from inductor impedance measurements. The curves $\mu_r(f)$ are then used as input of the PEEC-model. The magnetic coupling between $\mathbf{K_M}$ and the excitation electric currents $\mathbf{I_E}$ is interpreted in the form of partial elements represented by mutual inductances L_M [4]. The correlation between $\mathbf{K_M}$ and $\mathbf{I_E}$ currents was achieved by setting the boundary condition equation for the tangential component of magnetic field strength vector **H** at the points of the magnetic surface S_M. In the presence of magnetic materials, the standard PEEC system matrix then has to be extended with additional rows and columns, the elements of $\boldsymbol{\alpha}_{\mathbf{MM}}$ ($N_M \times N_M$), $\boldsymbol{\gamma}_{\mathbf{MI}}$ ($N_M \times N_J$) and $\mathbf{L_M}$ ($N_J \times N_M$) matrices, defined by the discretization of surface S_M into N_M panels.

$$\begin{bmatrix} A & -(R+j\omega L) & j\omega L_M \\ (j\omega P^{-1}+Y_L) & A^T & 0 \\ 0 & \lambda_{MI} & \alpha_{MM} \end{bmatrix} \begin{bmatrix} V \\ I \\ K_M \end{bmatrix} = \begin{bmatrix} V_S \\ I_S \\ 0 \end{bmatrix}. \quad (1)$$

IV. PEEC-Based Modelling of Filter Components

Following the PEEC methodology, the capacitors, inductors, and PCB tracks are represented by the corresponding PEEC cells such that their EM behavior is correctly modeled in the whole frequency range. In the following sub-sections, it is shown how the PEEC method can be employed to model EM properties of the EMI filter components in a very efficient way.

A. Modeling of Toroidal Inductors

In the developed PEEC-BIM method [4], the surface of the magnetic core is meshed into N_M panels and the EM influence of the core is represented by means of surface currents $\mathbf{K_{Mk}}$, $k = 1\ldots N_M$. In [5], it was proven by impedance and near-field measurements that the magnetic surface currents $\mathbf{K_{M\varphi}}$ are sufficient to describe the EM behavior of the toroidal cores with rectangular cross section, as typically selected for the design of practical EM filter inductors. Furthermore, by merging all panels at the circumferential angle θ_k, $n_{div\theta}$ magnetic current loops are defined carrying the unknown currents $\mathbf{I_M}$. In this way the PEEC-BIM method proposed in [4] is simplified so that the number of additional unknowns is decreased from N_M to $n_{div\theta}$ making the PEEC-BIM system matrix computationally less expensive. Specifically, the matrices $\boldsymbol{\alpha}_{\mathbf{MM}}$, $\boldsymbol{\gamma}_{\mathbf{MI}}$ and $\mathbf{L_M}$ are reduced to $\boldsymbol{\alpha}_{\mathbf{MMavg}}$ ($n_{div\theta} \times n_{div\theta}$), $\boldsymbol{\gamma}_{\mathbf{MIavg}}$ ($n_{div\theta} \times N_J$) and $\mathbf{L_{Mavg}}$ ($N_J \times n_{div\theta}$) matrices.

In Fig. 2, the PEEC-BIM model of a toroidal core is descriptively presented showing $n_{div\theta}$ magnetic current loops and two excitation windings in series connection, i.e. the DM winding configuration of a single phase CM inductor. The winding arrangement determines the nature of the fictitious magnetic currents; the strength of these currents is higher on the parts of the core covered with the windings, and they are proportional to the core permeability. Consequently, the PEEC model of an inductor consists of two parts: windings represented by a set of cylindrical PEEC cells and the magnetic core. By using the PEEC-BIM coupled method, it is shown that the strength of $\mathbf{K_M}$ is higher at the core regions covered by the winding and the $\mathbf{K_M}$ distribution determines the stray field of the inductor.

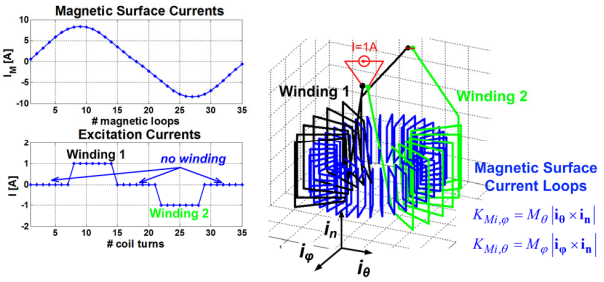

Fig. 2. Magnetic current loops $n_{div\theta} = 35$; two non-uniform windings (2×7 turns, i.e. DM configuration of a single-phase CM inductor).

The verification of the presented PEEC model was performed by measuring the impedances of the observed CM and DM inductors with the following specifications:

- *CM_1*: *VAC* VITROPERM 500F W380 nanocrystalline core [14], a single-phase 2×7 turns winding arrangement, wire diameter 1.4 mm; the complex permeability curves, ($\underline{\mu}(f) = \mu'(f) - j\mu''(f)$), are extracted from the measured impedance of an inductor with an uniform winding with 5 turns.
- *DM_1*: *Micrometals* T94-26 iron-powder core [15], uniform winding arrangement with 12 turns, wire diameter 1.4 mm; the relative permeability characteristic $\mu_r(f)$ of the core is taken from the datasheets.

The PEEC-based models of the CM and DM inductors are implemented in a simulation tool called "GeckoEMC" [16] as shown in Fig. 3. The comparison between the PEEC-based simulation and the impedance measurement results for the CM_1 and DM_1 inductors is presented in Fig. 4. The measurements were performed by means of an impedance analyzer, operating in the range from 40 Hz up to 110 MHz. For better PEEC simulation results at higher frequencies above 10 MHz more

accurate measurements of the permeability $\mu_r(f)$ would be needed.

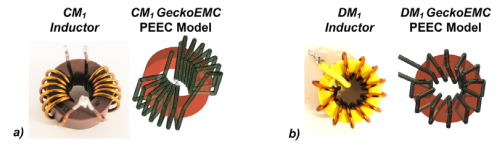

Fig. 3. Physical realization and corresponding 3D PEEC model (implemented in GeckoEMC) of toroidal inductors: a) CM_I b) DM_I.

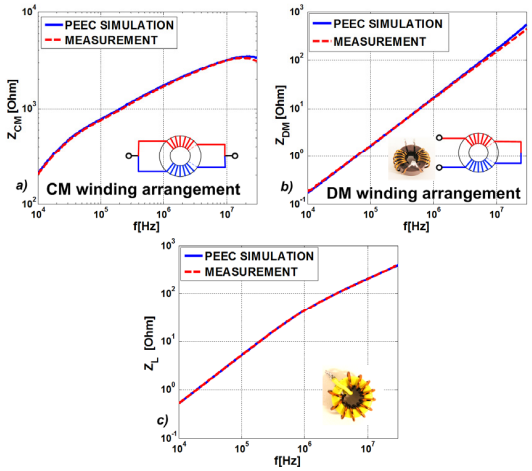

Fig. 4. Comparison of the impedance of the PEEC modeled inductors with measurements, for: a) DM / b) CM winding configurations of a single-phase CM_I inductor, and c) a DM_I inductor with a uniform winding.

B. *Modeling of Capacitors*

At higher frequencies starting from a few hundred kilohertz, capacitors must be represented by the equivalent series inductance (*ESL*), the equivalent series resistance (*ESR*), and the nominal capacitance *C*. Concerning the EM coupling, the current path through a capacitor determines the *ESL* which is strongly dependent on the length of the connectors. As the real structure of a capacitor is quite complicated, the PEEC model of capacitors is based on the homogenization method [10, 11, 17], keeping the same external geometrical properties. The resulting PEEC model of a capacitor is shown in Fig. 5.

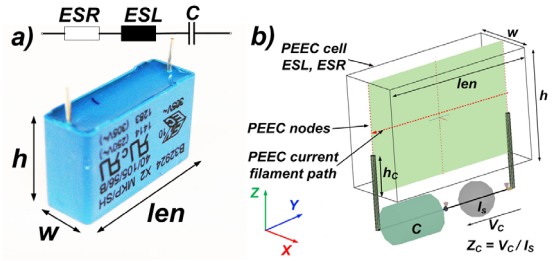

Fig. 5. a) Real capacitor and its equivalent electrical model; b) 3D PEEC model of the capacitor in GeckoEMC.

The capacitor is modeled by a PEEC cell with the same physical dimensions length (*len*), width (*w*) and height (*h*) as the real capacitor and 3*N* PEEC nodes in order to model a non-uniform current distribution in the y-cross section between the two connectors (Fig. 5b). The capacitive behavior is described by adding the capacitance *C* in series to the current path (y-direction in Fig. 5b) while the properties of the PEEC cell, the specific resistance (ρ), and the length of the connectors (h_C) are used to tune the PEEC model, i.e. to achieve the correct self-impedance Z_C of the capacitor. The PEEC based simulation of the capacitor was verified for two different capacitors with the following specifications:

- C_{DMI}: EPCOS X2 1.0 uF 305 VAC: *ESR* = 39 mΩ, *ESL* = 15 nH, *C* = 1 µF; h_C = 7.6 mm, ρ = 6900 S/m; [18]
- C_{CMI}: EPCOS X1/Y1 4.7 nF 250 VAC: *ESR* = 0.411 Ω, *ESL* = 11 nH, *C* = 4.7 nF; h_C = 4.5 mm, ρ = 900 S/m; [18].

The PEEC simulation results, the measured impedance Z_C and the equivalent electrical model of a C_{DMI} capacitor are shown in Fig. 6.

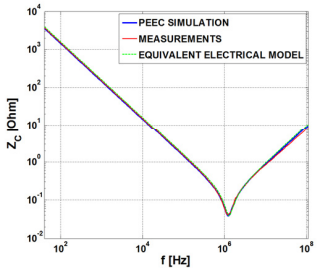

Fig. 6. Comparison of the impedance of the PEEC-modeled capacitor with measurements (C_{DMI}).

C. *Modeling of PCB Tracks*

PCB tracks can be represented by rectangular PEEC cells of same width, length and thickness as the real PCB tracks. The EM behavior of a PCB track is then modeled by the current filaments defined by the discretization of the cell volume. The PEEC model of PCB tracks and the PEEC capacitor model were verified by the measurements of the EM coupling between two loops including two C_{DMI} capacitors as shown in Fig. 7. The good agreement between the PEEC simulation and the measurements of the transfer function, i.e. V_{IND}/V_{IN} the induced voltage in the second loop due to the injected voltage in the first loop, is shown in Fig. 7b). The measurements were performed by means of a network analyzer, operating in the range from 100 kHz up to 1.8 GHz (see Section V).

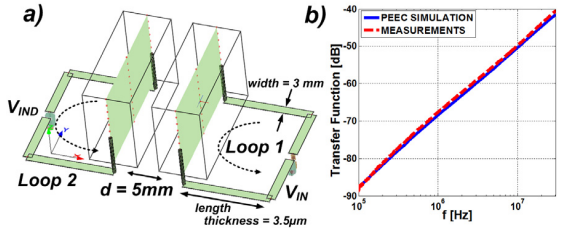

Fig. 7. a) EM coupling of Loop 1 with Loop 2 including two C_{DMI} capacitors at 5 mm distance; b) PEEC simulation vs. measurements of the transfer function, V_{IND}/V_{IN}, from Loop 1 to Loop 2.

V. PEEC-BIM EMI Filter Modeling – Verification

To verify the PEEC modeling approach for a full EMI filter structure, the PEEC simulation of a filter transfer function was compared to corresponding measurements for several EMI filter circuits. The real components were modeled by PEEC 3D models as presented in Section IV.

A. Measurement Setup

The measurements of filter transfer function were performed using two devices with different operating frequency ranges (f_{MIN}, f_{MAX}):

- Agilent HP4396A network analyzer with an operating frequency range of (100 kHz, 1.8 GHz)
- OMICRON Bode 100 vector network analyzer, with an operating frequency range of (10 Hz, 40 MHz).

In particular, the verification in the lower frequency range up to approximately 20 MHz was correctly covered by the Bode 100 vector network analyzer while better measurement results at higher frequencies were achieved with the HP4396A network analyzer. Two measurement setups are presented respectively in Fig. 8 and Fig. 9.

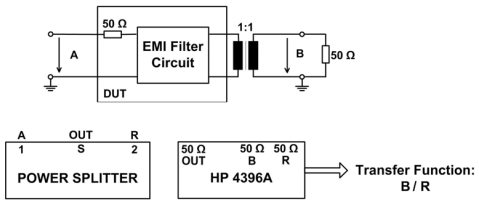

Fig. 8. Measurement setup with network analyzer HP 4396A using a power splitter to generate the reference signal, *R*.

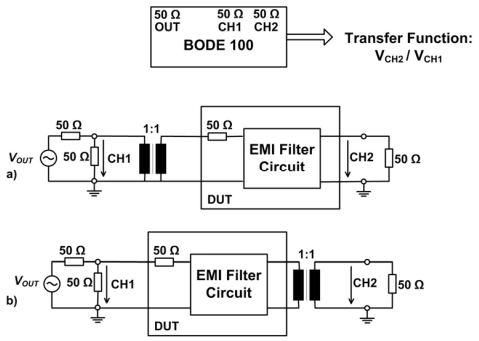

Fig. 9. Measurement setup with Bode 100 with the external connection of both channels CH1 and CH2 terminated with 50 Ω and the transformer placed at: a) the input; b) the output side.

The DUT block represents the measured EMI filter circuit with an additional series resistor of 50 Ω soldered directly onto the PCB in order to match the 50 Ω output resistance of the network analyzer. This additional resistor is included in the PEEC 3D simulation as y-element (see Fig. 1). In the measurements, the input (A, CH1) and the output terminals (B, CH2) are terminated with 50 Ω resistors to ground and hence a transformer with 1:1 transfer ratio has to be used for galvanic isolation of the input and/or the output sides. This enables correct measurement of the filter transfer function without short-circuiting the series impedance in the ground path across the measurement equipment and additionally helps to reduce the shield currents in the caoxial cables. However, in the PEEC simulation environment, the transfer function of the EMI filter is modeled as the ratio between input and output voltages while setting the voltage probes directly at the input and output terminals of the DUT, so that the transformer is simulated as an ideal component. Accordingly, in order to achieve a good matching between the simulation and measurement results, a transformer exhibiting the lowest influence on the frequency characteristics of DUT has to be used. As transformers are typically design for special applications and do not show good EM behaviour for low (LF) and high (HF) frequencies at the same time, the parasitic effects introduced by the transformer cannot be completely removed from the measurements and thus, differences between the PEEC simulation and the measurements can be observed, which is shown in the next subsections. For the connection between the DUT terminals and the measurement device, BNC connectors and matched 50 Ω coaxial cables are used keeping the minimum length of cables in order to reduce HF parasitic effects. The calibration of the measurement setups is performed for open and/or short circuited DUT terminals.

B. Modeling of EMI Input Filter Structures

To demonstrate the PEEC modeling capability for a virtual design of a full EMI filter, an EMI filter circuit (C-L-C structure) as depicted in Fig. 10a) is used. The equivalent inductance of the C-L-C circuit is the leakage inductance of a single phase CM_1 inductor. The PCB tracks are manufactured as the top layer and the copper (ground) plane, GP, as bottom layer of a PCB.

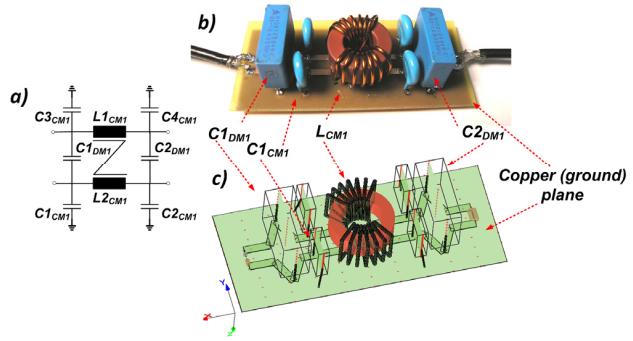

Fig. 10. a) Schematic and b) photo of the C-L_{CM}-C filter with four C_{CMI} capacitors to the ground plane, two C_{DMI} capacitors, a single- phase CM_1 inductor L_{CMI} and 35 µm PCB tracks; c) GeckoEMC 3D model.

The filter transfer function is measured using the network analyzer. The copper layer behaves as floating ground plane in the measurement setup. The measurements and the PEEC simulation results of the EMI filter transfer function are given in Fig. 11a) for frequencies from 100 kHz up to 30 MHz. The PEEC simulation returns the transfer function which models quite accurately the measured filter attenuation characteristic observing all three resonant frequencies. The influence of the transformer at the filter output is visible for frequencies above

20 MHz. The first resonance frequency at 135 kHz nicely matches with the first resonant frequency of the ideal filter which is due to the L_{CMI} - C_{DMI} resonant circuit; the second resonance at 1 MHz results from C_{DMI} - L_{PCB} - ESL (C_{DMI}); and the third resonance at 14 MHz is a result of the currents through the C_{CMI} capacitors connected to the copper plane. The PEEC simulation results of the EMI filter without C_{CMI} capacitors are shown in Fig. 11b). Namely, the PEEC based simulation enables a prediction of EMI filter performance distinguishing the EM influence of all components on the overall EMI filter HF behavior.

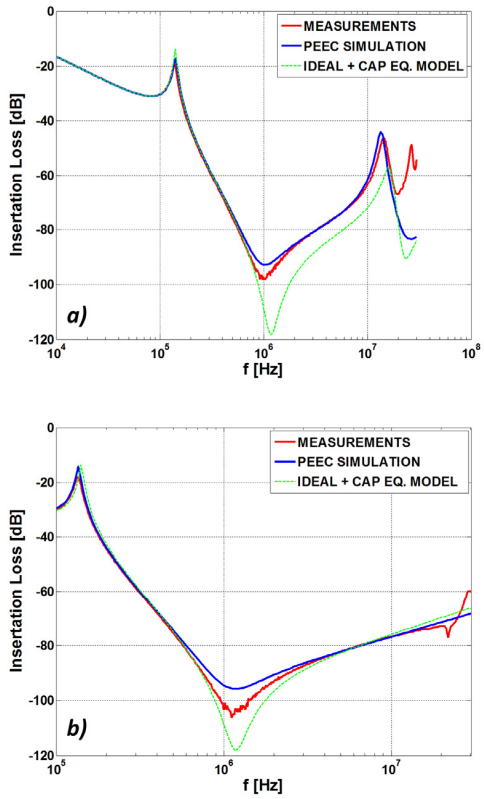

Fig. 11. Comparison between PEEC simulation, measurement results and the ideal characteristic of the EMI filter (Fig. 10) transfer function: a) with, b) without C_{CMI} capacitors.

To demonstrate an impact of the 1:1 transformer on the measurement results, the C-L-C filter structure with two *DMI* inductors (Fig. 12) was measured using the Bode 100 analyzer employing two different transformers: (1) a commercial transformer (a wide-band transformer, CoilCraft WB1010-1) [19] and (2) a custom made transformer (10 turns of twisted pair on VITROPERM 500F W914 core, wire diameter 0.2 mm [14]). The custom made transformer was built with approximately two times lower parasitic capacitance between the primary and the secondary windings (10 pF). The measured and the PEEC simulated transfer functions with and without *CM* capacitors are presented in Fig. 13 a) and b), respectively. Accordingly, the custom made transformer shows better performance and introduces less parasitic effects in the HF range above 20 MHz. Therefore, special care must be taken in designing the measurement setup in order to measure the real filter characteristics and reduce the parasitic measurement effects which cannot be totally removed via calibration.

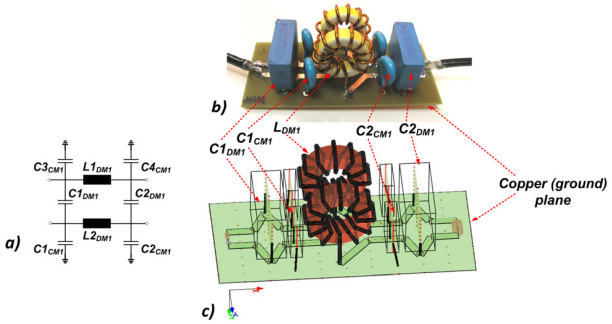

Fig. 12. a) Schematic and b) photo of the C-L_{DM}-C filter with four C_{CMI} capacitors to the ground plane, two C_{DMI} capacitors, two DM_I inductors L_{DMI}, and 35 µm PCB tracks; c) Gecko EMC 3D model.

C. *Modeling of Two-Stage EMI Filter*

The developed PEEC modelling approach is further used to predict the attenuation of a two-stage EMI filter (C-L-C-L-C structure), as shown in Fig. 14, with an arrangement and selection of filter components as typically applied in EMI input filters of the power converter systems [20].

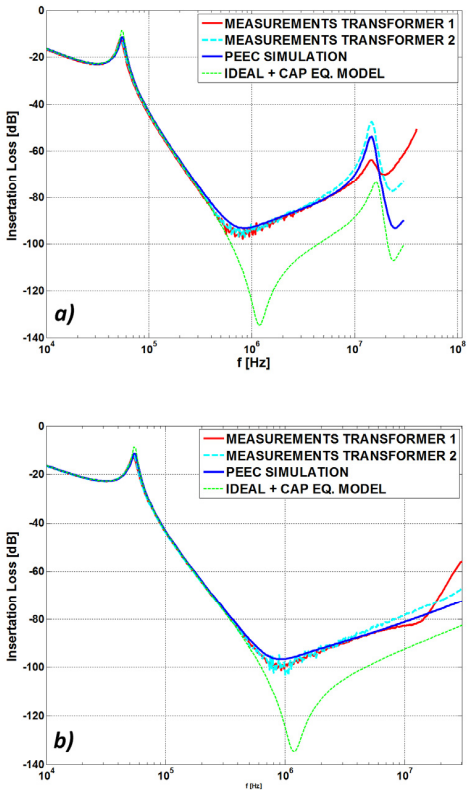

Fig. 13. Comparison between PEEC simulation, two measurement results and the ideal characteristic of the EMI filter (Fig. 12) transfer function: a) with b) without C_{CM} capacitors; transformer1 - commercial transformer, transformer 2 - custom made transformer.

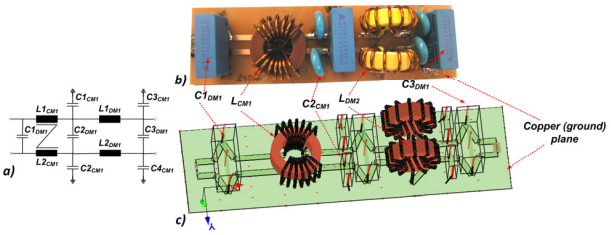

Fig. 14. a) Schematic and b) photo of the C-L_{CM}-C-L_{DM}-C filter with C_{CMI} capacitors to ground plane, three C_{DMI} capacitors, two DM_I inductors L_{DMI}, a single-phase CM_I inductor L_{CMI} and 35 µm PCB tracks; c) Gecko EMC 3D model.

The comparison between the simulated and the measured transfer functions (using the Bode 100 analyzer) are given in Fig. 15 a) and b).

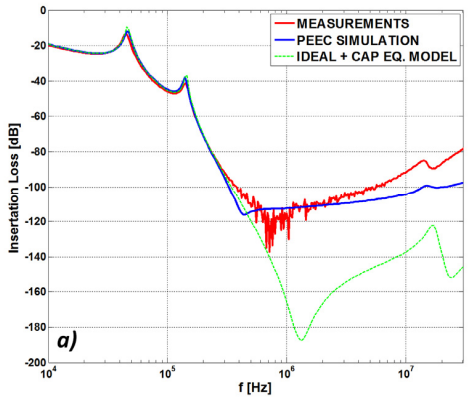

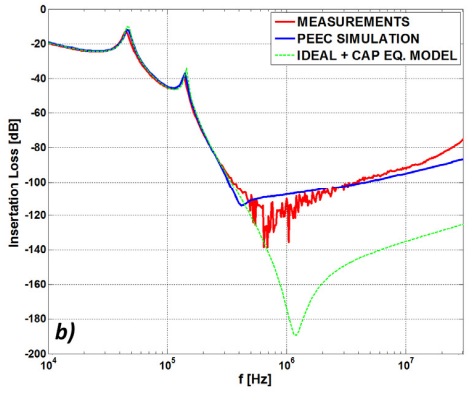

Fig. 15. Comparison between PEEC simulation, two measurement results and the ideal filter characteristic of the EMI filter (Fig. 16) transfer function: a) with b) without C_{CMI} capacitors.

In the case of CM capacitors connected to the copper (ground) plane, four resonances in the transfer function can be observed: f_{R1} = 45 kHz (due to C_{DMI} - L_{DM}), f_{R2} = 140 kHz (due to C_{DMI} - L_{CM}), f_{R3} = 140 kHz (due to C_{DMI} - L_{PCB} - ESL_{CDMI}) and f_{R4} = 15 MHz (due to the current through C_{CMI}). The modeled two-stage EMI filter introduces a significant attenuation of approximately -120 dB which cannot be accurately measured using the measurement equipment. Therefore, a mismatch between the measured and the simulated transfer functions is visible at attenuation levels below -100 dB and at frequencies above 10 MHz due to the HF influence of the transformer. However, the HF behaviour of the observed filter circuit is accurately modeled with a deviation of less than 10 dB by the PEEC-based method, which in turn can be used as a 3D modelling environment that enables to find an optimal filter configuration and to identify negative EM coupling effects between the components.

D. *Modeling of PFC EMI Filter*

As third example for the model verification, a power factor correction (PFC) input filter stage, shown in Fig. 16, is chosen. The same PCB layout as in the previous example of the two-stage filter was used, so that the DM_I inductor, L_{DMI} represents a boost inductor and the C - L_{CM1} - C part a single-stage input filter [21, 22]. A good agreement between the PEEC simulation and the measurement results was achieved in the whole frequency range of interest (Fig. 17) using the Bode 100 analyzer.

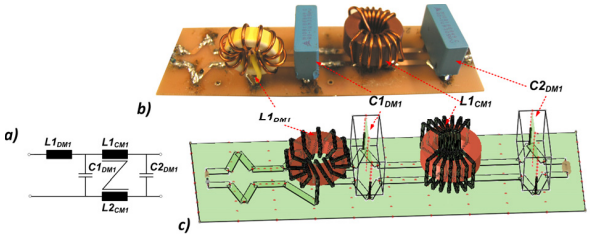

Fig. 16. a) Schematic and b) photo of the L_{DM}-C-L_{CM}-C filter with a boost DM_I inductor L_{DMI} and the single-phase filter stage including CM_I inductor L_{CMI} and two C_{DMI} capacitors; c) GeckoEMC 3D model.

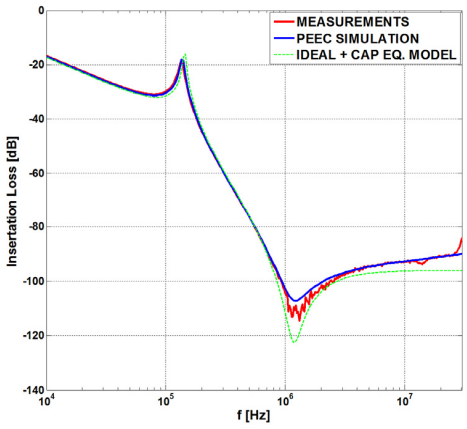

Fig. 17. Comparison between PEEC simulation, two measurement results and the ideal filter characteristic of the EMI filter (Fig. 19) transfer function.

VI. PEEC-BIM Simulation Performance

The mesh of the magnetic surface into N_M panels determines the computational complexity and accuracy of the implemented PEEC-BIM method. The simulations were

performed on standard PCs with a 64-bit Win OS, and a CPU clock frequency of 2.4 GHz. The PEEC simulations of the filter circuits presented in Section V take several minutes depending on the number of magnetic elements i.e. magnetic cores to be modeled. The magnetic core of L_{CMI} inductors was modeled by $n_{div\theta}$ = 35 magnetic current loops while in the case of L_{DMI} inductors the mesh of $n_{div\theta}$ = 24 was applied. The good results of the verification described in Section V point out that the PEEC discretization allows accurate 3D modeling of power electronic systems with significantly less computational effort than required for an equivalent FEM analysis.

VII. Future Research

In the course of future research, the following topics have to be examined in more detail: (1) designing an optimal measurement setup to minimize the influence of measurement equipment parasitic effects, (2) PEEC-based modeling of CM current paths, (3) PEEC modeling of electrostatic shielding layers; (4) PEEC modeling of E-shaped magnetic cores; (5) optimization procedure calculating the optimum component placement (minimizing coupling effects of given EMI filter circuits in a given restricted construction space).

VIII. Conclusion

After the implementation and experimental verification of the individual PEEC component models for inductors, capacitors, PCB tracks, and their mutual coupling, single-stage C-L-C filters were modeled and investigated including their LF and HF characteristics. Furthermore, it was shown that good agreement between measurements and PEEC simulation results of the filter transfer function can be achieved for different single-phase single/two-stage EMI input filter circuits, employed to suppress conducted CM and/or DM noise levels in the real power electronics systems. To distinguish the parasitic effects introduced by the measurement setup from the frequency behavior of the device under test and to accurately verify the proposed PEEC modeling approach in the range from low frequencies up to 30 MHz, the verification was performed by two measurement devices, an Agilent HP4396A network analyzer and an OMICRON Bode 100 vector network analyzer. It was shown that the impact of the component placement, i.e. PCB layout, on the resulting filter attenuation can be accurately predicted by the developed PEEC-based modeling method finally implemented in the simulation tool GeckoEMC. Accordingly, such EMC modeling environment represents a highly useful tool for virtual prototyping of EMI filters and other power converter systems, speeding up the design process and allowing engineers to build good EMC designs without wide practical experience.

References

[1] R. Redl, "Electromagnetic enviromental impact of power electronic equipment," in *Procedings of the IEEE*, vol. 89, no. 6, pp. 926-938, Aug. 2001.

[2] A. Lissner, E. Hoene, B. Stube, and S. Guttowski, "Predicting the influence of placement of passive components on EMI behavior," in *European Conf. on Power Electronics and Applications (EPE),* pp. 1-10, 2007.

[3] A. Muesing, J. Ekman, and J. W. Kolar, "Efficient calculation of non-orthogonal partial elements for the PEEC method," *Trans. on Magnetics*, vol. 45, no.3, pp. 1140-1143, Feb. 2009.

[4] I. Kovacevic, A. Muesing, and J. W. Kolar, "PEEC modeling of toroidal magnetic inductors in frequency domain," in *Int. Power Electronic Conf. (IPEC)*, pp. 3158-3165, 2010.

[5] I. Kovacevic, T. Friedli, A. Muesing, and J. W. Kolar, "A full PEEC model of EMI filter inductors in frequency domain," accepted for publication for COMPUMAG 2011, Sydney, Australia, July 2011.

[6] S. P. Weber, E. Hoene, S. Guttowski, and W. John, "Predicting parsitics and inductive coupling in EMI filters," in *IEEE Applied Power Electronic Conf. (APEC)*, pp. 1157-1160, 2006.

[7] S. Wang, F. Lee, D. Chen, and W. Odendaal, "Effects of parasitic parameters on EMI filter performance," *IEEE Trans. on Power Electron.*, vol. 19, no. 3, pp. 869–877, May 2004.

[8] S. Wang, F. Lee, and W. Odendaal, "Characterization and parasitic extraction of EMI filters using scattering parameters," *IEEE Trans. on Power Electron.*, vol. 20, no. 2, pp. 502–510, March 2005.

[9] E. Hoene, A. Lissner, S. Weber, S. Guttowski, W. Johan, and H. Reichl, "Simulating electromagnetic interactions in high power density inverters," in *IEEE Power Electronic Specialists Conference* (*PESC)*, pp. 1665-1670, June 2005.

[10] T. De Oliveira, J-L. Schanen, J-M. Guichon, and L. Gerbaud, "Automatic layout optimization of an EMC filter," in *IEEE Energy Conversion Congress (ECCE)*, pp. 2679-2685*, Sept.* 2010.

[11] T. De Oliveira, J-M. Guichon, J-L. Schanen, and L. Gerbaud, " PEEC models for EMC filter layout optimization," in *Inter. Conf. on Integrated Power Electronic Systems (CIPS)*, Paper 13.3, 2010.

[12] GeckoCIRCUITS, [Online]. Available: http://www.gecko-research.com/geckocircuits.html.

[13] D. M. Cook, The theory of the electromagnetic field, 1975, Prentice – Hall, Inc., Englewood Cliffs, New Jersey, pp. 289-324.

[14] Vacuumschmelze, Nanocrystalline VITROPERM – EMC Components, Vacuumscmelze GmbH. & Co., 2004

[15] Micrometals, [Online]. Available: http://www.micrometals.com.

[16] GeckoEMC, [Online]. Available: http://www.gecko-research.com/geckoemc.html.

[17] S-P. Weber, E. Hoene, S. Guttowski, W. John, and H. Reichl, "On coupling with EMI capacitors," in *IEEE Symposium on EMC (EMC)*, pp. 336-341, Aug. 2004.

[18] EPCOS, [Online]. Available: http:// www. epcos.com.

[19] CoilCraft, [Online]. Available: http://www.coilcraft.com.

[20] Schaffner*, Datasheets: Single Stage Filters*, [Online]. Available: http://www.schaffnerusa.com/.

[21] J. R. R Zientarski, J. R. Pinheiro, H. L. Hey, R. C. Beltrame, D. B. Candido, "A design methodology for boost inductor applied to PFC converters considering the core temperature rise and the conducted EMI noise," in *European Conf. on Power Electronics and Applications (EPE)*, pp. 1-10, Sept. 2009.

[22] L. Rosseto, S. Busso, and G. Spiazzi, "Conducted EMI issues in a boost PFC design," in *Intern. Telecom. Energy Conf.* (*INTELEC*), pp. 188-195, Oct. 1998.